Assimilation of sea ice motion in a Finite Element Sea Ice Model

K. Rollenhagen[1], R. Timmermann[1], T. Janjic[1], J. Schröter[1], S. Danilov[1]

August 4, 2008

[1] Alfred-Wegener-Institute for Polar and Marine Research, Bremerhaven, Germany

Abstract

A Finite-Element Sea-Ice Model (FESIM) is applied in a data assimilation study with the Singular Evolutive Interpolated Kalman (SEIK) Filter. The model has been configured for a regional Arctic domain and is forced with a combination of daily NCEP reanalysis data for 2-m air temperature and 10-m winds with monthly mean humidities from the ECMWF reanalysis and climatological fields for precipitation and cloudiness. We assimilate three-day mean ice drift fields derived from passive microwave satellite data. Based on multivariate covariances (which describe the statistic relationship between anomalies in different model fields), the sea-ice drift data assimilation produces not only direct modifications of the ice drift but also updates for sea-ice concentration and thickness, which in turn yield sustainable corrections of ice drift. We use observed buoy trajectories as an independent dataset to validate the analyzed sea ice drift field. A good agreement between modeled and observed tracks is achieved already in the reference simulation. Application of the SEIK filter with satellite-derived drift fields further improves the agreement. Spatial and temporal variability of ice thickness increases due to the assimilation procedure; a comparison to thickness data from a submarine-based upward looking sonar indicates that the thickness distribution becomes more realistic. Validation with regard to satellite data shows

that the velocity data assimilation has only little effect on ice concentration, but a general improvement of the ice concentration within the pack is still evident.

1 Introduction

Data assimilation in sea-ice models has been carried out for almost 20 years, but has largely been restricted to an analysis and optimization of ice concentration. A Kalman smoothing method has been applied by *Thomas and Rothrock* (1989, 1993) to assimilate passive microwave sea-ice concentration data in a simple sea ice model which was forced by optimally interpolated buoy drift fields. This work has been extended by *Thomas et al.* (1996) using a thermodynamic sea-ice model plus observed sea-ice motions, winds and concentrations to obtain and analyse spatial and temporal variations of Arctic sea-ice thickness distribution. A comparison with submarine-derived ice draft data revealed that the Arctic-wide thickness estimates agree well with the observations but underestimate spatial variability.

Data assimilation of microwave sea-ice concentration data with an Ensemble Kalman (EnKF) Filter in a general circulation model of the Arctic ocean has been presented by *Lisæter et al.* (2003). Experiments featured an improved sea ice concentration, but the effect on the ice thickness distribution was small.

Due to the lack of gridded data for sea-ice thickness observations, only very few studies with ice thickness assimilation have been conducted. In order to examine the potential for ice thickness assimilation in coupled sea-ice/ocean models, *Lisæter et al.* (2007) used synthetic CryoSat data in an EnKF setup. Their experiments illustrate that ice thickness observations can have a strong impact on modeled ice thickness estimates, but that an appropriate forcing is crucial. Specifically, it is shown that a stochastic wind forcing is important to correctly describe model errors.

Assimilation of sea-ice velocities so far mostly relies on OI or nudging schemes. The study of *Meier et al.* (2000) was the first attempt to assimilate sea-ice velocities into a large scale sea-ice model for the Arctic. They obtained an improved ice drift, but also unrealistic changes of the sea-ice thickness near the Greenland coast and the Canadian Archipelago and in the mass outflow through Fram Strait. Other studies (*Meier and Maslanik*, 2001a,b) have shown that the assimilation of sea-ice velocities is able to improve model estimates of buoy trajectories and synoptic events of Arctic sea-ice velocities. *Meier and Maslanik* (2003) further investigated effects of local conditions, namely proximity to the coast, sea-ice thickness and wind forcing, on Arctic remotely sensed, modeled and assimilated sea-ice velocities. *Arbetter et al.* (2002) combined satellite-derived and modeled sea-ice velocities in a large-scale Arctic sea-ice model to simulate the anomalous summer sea-ice retreat in 1990 and 1998.

In a recent study, *Dai et al.* (2006) analyzed the model sensitivity to ice strength parameterizations by assimilating sea-ice velocities. *Zhang et al.* (2003) conducted a hindcast simulation of Arctic sea-ice variations of the period 1992-1997 with a regional sea-ice ocean general circulation model where buoy and passive microwave sea-ice motion data are assimilated. The assimilation leads to an improved motion and substantially decreased stoppage which strengthened the ice outflow in the Fram Strait and enhanced ice deformation. *Lindsay et al.* (2003) have extended this work for a ten month period in 1997 and 1998.

In a series of twin experiments, *Dulière and Fichefet* (2007) and *Dulière* (2007) assimilated sea-ice concentration and velocities in a simplified and a full-physics model of the Arctic sea-ice pack with a modified OI algorithm. Their aim was to study to what degree the assimilation of sea ice velocity and/or concentration data improves the global performance and reduces errors in sea-ice thickness simulation. The results indicate that under certain conditions, depending on assimilation weights and type of model error, the sea-ice velocity assimilation improves the model performance. They suggest that when ice concentration is modified, conservation of (actual) ice thickness should be prefered to conservation of ice volume.

Another study with simultaneous assimilation of ice concentration and motion was recently presented by *Stark et al.* (2008). Here, the assimilation is able to significantly reduce the model errors in sea ice concentration and velocity, but has little effect on the ice thickness distribution. In contrast to the above-mentioned studies of Dulière, who use a optimally interpolated velocity fields for advection of sea ice thickness and concentration, *Stark et al.* (2008) introduced an additional stress term in the sea ice momentum balance. This so-called stress increment is not attributed to any specific physical process but represents an unkown combination of stresses that are required to obtain a new (corrected) sea ice velocity.

The assimilation of sea-ice drift is complicated by the fact that the inertia of sea ice is small compared to the effects of wind stress and internal ice strength. Although a progostic variable, determined from a differential equation, sea-ice drift in the model behaves very similar to a diagnostic quantity. With respect to the momentum balance, the system has very little memory beyond each model time step, making direct drift field corrections very short-lived. A single correction of the velocity field, even if it were perfect, has very little effect on the further evolution of the model state.

Ice-drift history, however, is stored in the sea-ice thickness and concentration distributions, and these distributions feed back to the velocity field. In this project, we use the singular evolutive interpolated Kalman (SEIK) filter (*Pham et al.*, 1998; *Pham*, 2001) to obtain the redistribution of sea ice. By considering the covariance of sea-ice thickness and drift as well as the covariance of sea-ice concentration and drift, the SEIK Filter is able to update the more conservative state variables "ice thickness" and "ice concentration" during the course of assimilation, which in turn leads to modifications of the large-scale sea-ice distribution. We use satellite-derived sea-ice velocities with the aim to improve model estimates not only of ice velocities but also of ice concentration and thickness. Independent datasets of ice drift, concentration, and thickness are used for validation.

We describe the numerical model, the assimilation procedure and the data used for assimilation and validation in Section 2. Results from experiments with and without velocity data assimilation are presented in section 3, followed by a discussion and conclusions.

2 Model, SEIK Filter and Data

2.1 FESIM

The Finite Element Sea Ice Model (FESIM) is the sea-ice component of the Finite Element Sea ice–Ocean Model (FESOM; *Timmermann et al.*, 2008). It is a dynamic-thermodynamic sea-ice model with the *Parkinson and Wash-*

ington (1979) thermodynamics. The model includes a prognostic snow layer (*Owens and Lemke*, 1990) accounting for the effect of snow-ice conversion due to flooding (*Leppäranta*, 1983; *Fischer*, 1995). Heat storage in the ice and the snow is neglected, so that linear temperature profiles in both layers are assumed (so-called zero-layer approach of *Semtner* (1976)). Prognostic variables are the ice volume per unit area (also called mean ice thickness) h_i, the snow volume per unit area (mean snow thickness) h_s, the ice concentration A and the ice (and snow) drift velocity $\mathbf{u}_i$.

For the computation of ice (and snow) drift, the model applies the elastic-viscous-plastic rheology of *Hunke and Dukowicz* (1997). Sea surface tilt force is computed using the dynamic elevation (sea surface height) from the ocean module. Model parameters have been chosen following studies with other stand-alone Arctic sea ice models (*Kreyscher*, 1998; *Harder and Fischer*, 1999; *Lieser*, 2004; *Martin*, 2007). The ice strength is parameterized as

$$P = P^{*} h_i \, \mathrm{e}^{-C(1-A)} \tag{1}$$

(*Hibler*, 1979) with a constant $C = 20$ and an ice strength parameter $P^{\star} = 15\,000\ \mathrm{Nm}^{-2}$. Further information about the model is given by *Timmermann et al.* (2008).

Here, we run the model in a decoupled mode which neglects the horizontal advection (and diffusion) of oceanic temperature and salinity and turns the model into a standalone sea ice model which is locally coupled to a onedimensional ocean mixed layer/turbulence model for every node of the computational mesh. For parameterization of turbulent fluxes of heat and salt between the ocean interior and the ice-ocean interface we use the vertical turbulence/convection parameterization from FESOM's ocean component. It is based on a modified version of the *Pacanowski and Philander* (1981) mixing scheme. We use it with a maximum diffusivity/viscosity of 0.01 m^2/s, which is also applied in case of a statically unstable stratification (i.e. negative Richardson number).

While this approach retains a fully interactive flux coupling for temperature and salinity, ocean currents need to be prescribed to ensure a correct computation of the sea-ice momentum balance and of the Richardson number in the vertical mixing scheme.

2.2 Data Assimilation

SEIK Filter The SEIK Filter (*Pham et al.*, 1998; *Pham*, 2001) represents a sequential data assimilation method that combines, at the times when observations are available, the (predicted) model state estimate with observations. The SEIK filter is an ensemble-based Kalman filter that exploits the low rank of the ensemble-derived covariance matrix to obtain an efficient analysis scheme for incorporating the observational information. The filter algorithm can be subdivided into four phases: initialization, forecast, analysis and re-initialization. The sequence of forecast, analysis and re-initialization is repeated.

Initialization The initial model state estimate $\mathbf{x}_0^a$ is obtained from the end of a model-only spinup simulation. The initial covariance matrix $\mathbf{P}_0^a$ is estimated from monthly mean anomalies of the last ten years (1990-1999) of the same simulation using singular value decomposition of the ensemble-derived covariance matrix. The matrix $\mathbf{P}_0^a$ is of rank r; its r largest eigenvalues are equal to the largest eigenvalues of the ensemble-derived covariance matrix. With these initial estimates, a random ensemble of size $N = r + 1$ is generated using minimum second order exact sampling (*Pham*, 2001). Ensemble mean and covariance matrix represent $\mathbf{x}_0^a$ and $\mathbf{P}_0^a$ exactly.

Forecast The evolution of each ensemble member is forecasted with the full nonlinear model. The model operator $\mathbf{M}_{k-1,k}$ represents the FESIM integration from time t_{k-1} to time t_k:

$$\mathbf{x}_k^{f(l)} = \mathbf{M}_{k-1,k}\mathbf{x}_{k-1}^{a(l)}. \tag{2}$$

The superscript 'f' denotes the forecast while 'a' denotes the analysis. Due to different $\mathbf{x}_{k-1}^{a(l)}$ the model integration produces different $\mathbf{x}_k^{f(l)}$ which allow for an estimate of the forecast error covariance $\mathbf{P}_k^f$ at time t_k.

Analysis The SEIK Filter analysis is based on a description of $\mathbf{P}_k^f$ in terms of the ensemble states that allows for an easy calculation of $\mathbf{P}_k^a$ in its factorized form. By updating the forecast field (which is given by the mean of the forecast ensemble), the analysis of the SEIK Filter yields a new state estimate. This update can be expressed using the equation:

$$\mathbf{x}_k^a = \mathbf{x}_k^f + \mathbf{P}_k^a \mathbf{H}_k^T \mathbf{R}_k^{-1} \left(\mathbf{y}_k^o - \mathbf{H}_k \mathbf{x}_k^f \right) . \tag{3}$$

Here, $\mathbf{H}_k$ is the operator which interpolates the model state to the observation location, $\mathbf{R}_k$ is the observation error covariance matrix, and the vector $\mathbf{y}_k^o$ represents the observations. A forgetting factor < 1.0 leads to an increase of the estimated variances of the model state and is chosen to maintain a robust rms error approximation. It is used for calculation of the analysis error covariance (see *Pham* (2001) for details).

Re-Initialization In order to proceed with the filter sequence, a new ensemble of size $N = r + 1$ is generated around the updated state $\mathbf{x}_k^a$ using the corresponding covariance matrix $\mathbf{P}_k^a$. As in the initialization step, second order exact sampling is used to have the mean of the ensemble equal to $\mathbf{x}_k^a$ and the ensemble-derived covariance equal to $\mathbf{P}_k^a$ exactly.

2.3 Observations

For velocity data assimilation, we use 3-day mean merged SSM/I and Quikscat ice motion data provided by the French ERS Processing and Archiving Facility CERSAT (*Ezraty and Piollé*, 2004a). These data were obtained through the National Snow and Ice Data Center (NSIDC) on the standard NSIDC grid of 12.5 km $\times$ 12.5 km, but the data only have a resolution of 62.5 km $\times$ 62.5 km. Naturally, these data have a much better spatial coverage than buoy motion data, but the number of available data still varies with time. Most substantial of all, there are no data from 1 May to 30 September.

The estimated uncertainty or error of these observations is derived from the position uncertainty arising from the nominal pixel size of the grid and an additional uncertainty due to fact that the actual pixel size depends on latitude (*Ezraty and Piollé*, 2004b). In addition to that, a typical drift observation error for the merged 3-day mean drift components amounts to approximately 1.4 to 1.6 $\mathrm{cm\,s^{-1}}$ (depending on the actual drift) which corresponds to an ice speed error of 1.97 to 2.26 $\mathrm{cm\,s^{-1}}$ (*Ezraty and Piollé*, 2004a).

As an independent dataset for validation, we use sea-ice drift trajectories from the International Arctic Buoy Programme (*Rigor*, 2002). For a consistent comparison, we compute drift velocities for time periods of 3 days. Most buoy localizations yield a position error of less than 300 m (*Ortmeyer* *and Rigor*, 2004). A typical distance error is about 2.2 km for three days, which corresponds to a velocity error of approximately 8 $\mathrm{mm\,s^{-1}}$.

Sea-ice concentration data for validation of data assimilation results were obtained from the CERSAT data base. They were derived from the 85 GHz brightness temperature maps processed with the Artist Sea Ice algorithm (*Kaleschke et al.*, 2001; *Kaleschke*, 2003) and mapped onto the NSIDC 12.5 km $\times$ 12.5 km grid. The observational error for these data is estimated to be 5 to 10 % of sea-ice concentration depending on the season and location (*Kaleschke*, 2003; *Comiso et al.*, 1997).

Evaluation of sea ice thickness in this study relies on measurements of Arctic sea-ice drafts by US Navy submarines. These submarines are equipped with an upward looking sonar (ULS) that continually measures the distance to the sea-ice bottom while a pressure sensor provides the distance to the sea surface (*Rothrock et al.*, 2003). Sea-ice draft is then defined by the difference between these distances. The data were processed by the Polar Science Center at the University of Washington and were obtained by digitizing analog paper charts (*Wensnahan and Rothrock*, 2005). After the US Navy released these data, they became available through the NSIDC (*NSIDC*, 1998, updated 2006). The data are all located outside the Exclusive Economic Zones in the central Arctic. The position information is accurate to within $1/12^\circ$ which corresponds to an accuracy of approximately 5.6 km and is less than the FESIM grid resolution. The date is given within a 10-day leg (*Wensnahan*, 2006). A submarine cruise of the year 2000 has been chosen for comparison with assimilation results. The simple relation (neglecting a possible snow cover)

$$h_{\mathrm{ice}} = d\,\frac{\rho_{\mathrm{water}}}{\rho_{\mathrm{ice}}} \tag{4}$$

is used to compute ice thickness h_{ice} from draft d, assuming constant densities of sea ice ρ_{ice} and ocean ρ_{water}.

2.4 Experimental set-up

2.4.1 Configuration and forcing

The model is configured for the region of the Arctic Ocean and the neighboring Nordic Seas (Figure 1) on an almost regular 1/4° grid. Atmospheric forcing fields consist of daily NCEP reanalysis data for 2-m air temperature and 10-m wind (*Kistler et al.*, 2001; *Kalnay et al.*, 1996), combined with monthly mean humidity data from the ECMWF reanalysis (*Gibson et al.*, 1997) and climatological means derived from observations for precipitation (*Vowinckel and Orvig*, 1970) and cloudiness (*Ebert and Curry*, 1993). To obtain the ocean currents that need to be prescribed in the uncoupled simulations, the model was run in coupled mode for 18 years. Ocean velocities were averaged over the last 15 years of the coupled integration.

A model spinup has been performed for the years 1950-2000. Both reference simulation and assimilation experiments start from 30 September 2000, using results from the spinup as initial conditions. Since we are mainly interested in an improved description of seasonal ice thickness redistribution, data assimilation is applied for the months October to December, i.e. the transition from autumn to winter.

2.4.2 The assimilation set-up

In the SEIK Filter framework established here, the state vector $\mathbf{x}_k^a$ includes the prognostic variables sea-ice drift velocity $\mathbf{u}_i$, mean ice thickness h_i, ice concentration A, mean snow thickness h_s, and ocean temperature T and salinity S. The initial covariance matrix $\mathbf{P}_0^a$ is estimated from the variability of a model-only experiment. An ensemble of 23 state realizations is used in the forecast phase.

Adapted to the interval of drift observations, ensemble forecasts are computed for three days. Every third day the mean state is determined and the analysis is performend, followed by the resampling step (see Section 2.2). This cycle is repeated throughout the full period of assimilation.

Compared to the variability on the three-day timescale (which is the interval between two SEIK analyses), the initial covariances between sea-ice velocity and thickness/concentration, derived from monthly mean fields, are overestimated. Within a few assimilation steps, the ensemble integration reduces covariances substantially.

A series of sensitivity experiments has been conducted to find an appropriate value for the forgetting factor ρ (suggested by *Pham* (2001)). We found that for the present set-up best results are obtained with $\rho = 0.8$.

Due to the statistical nature of the process, small negative values for ice thickness and concentration can be produced during the re-initialization phase. These are locally replaced by zero.

3 Results

3.1 Ice Motion

A comparison with observed sea-ice velocities indicates that realistic drift fields are obtained in the model-only simulation already. The assimilation procedure improves the agreement with observations even further. Specifically, the comparison to buoy drift trajectories (Figure 2), which have not been used during the assimilation procedure and represent an independent dataset, shows a good convergence of the simulated buoy trajectory towards the true buoy trajectory in most (although not all) cases. The correlation between simulated and observed velocities increases from 0.43 (without assimilation) to 0.57 (with assimilation). On first sight, the progress and the correlations do not appear particularly high; however, it has to be kept in mind that even the correlation between SSM/I velocities (which are used for assimilation) and buoy velocities (which are used for validation) is only 0.67. Differences between the two observational datasets are obviously far from being negligible, and it is only natural that no perfect agreement with the observed buoy tracks can be achieved here. The root-mean-square error (rmse) with respect to buoy derived sea-ice speed is reduced from 0.056 m/s (without assimilation) to 0.051 m/s (with assimilation). With respect to the satellite data, sea-ice speed rmse is reduced from 0.043 m/s (without assimilation) to 0.037 m/s (with assimilation).

Time series of three-day mean velocities derived from buoy data, SSM/I data, reference simulation and assimilation results (Figure 3) reveal a strong but not perfect correlation between buoy and SSM/I data. Assimilation improves ice velocities; most of the observed minima and maxima are captured rather realistically. The sea-ice velocity improvement increases with ongoing assimilation - we will show later that this is due to a progressive adjustment of sea-ice concentration and thickness. While the top velocities are not captured at the beginning of the assimilation, the differences between the maximum values decrease within a few weeks - which indicates a rather swift adjustment process.

A typical example for the correction of drift patterns through assimilation is presented in Fig. 4. The sea-level pressure (SLP) fields (top left panel) from the NCEP reanalysis features a pronounced anticyclone located over the East Siberian Sea and the adjacent sector of the Arctic Basin. Consequently, a strong westward drift in the Beaufort, Chukchi and East Siberian Seas and a pronounced Transpolar Drift Stream (TDS) are the main features of the large-scale sea-ice drift field. Given that the NCEP reanalysis 10-m wind is strongly connected with the SLP pattern, it is not surprising that simulated drift in the model-only experiment (Fig. 4, top right) follows the SLP pattern very closely as well. In the observed drift pattern (Fig. 4, bottom left), however, the center of the anticyclonic sea-ice drift is located further to the west in the Beaufort Sea, close to the coasts of Canada and Alaska. Using the observations as a reference, the westward ice drift north of Greenland and the Canadian Archipelago is obviously overestimated in the model-only simulation. Furthermore, we find the TDS transporting ice mainly from Laptev Sea to Fram Strait in the observed drift field, while in the model-only simulation, the Laptev Sea ice only feeds the recirculation in Canada Basin and the ice exported through Fram Straits originates from Kara Sea. Given that ice thicknesses can differ significantly between Kara and Laptev Sea, the difference in transport patterns is bound to affect Fram Strait ice export rates.

The simulation with ice velocity data assimilation (Fig. 4, bottom right), features a drift pattern that is much closer to the observations. The analysis corrects the location of the center of the gyre, partly redirects the TDS, and reduces the recirculation north of Greenland. Instead of simply replacing the modeled drift field with the observations, which is bound to violate the model's dynamic balances, the Kalman filter finds a consistent state that considers both the model estimate and the observations.

Further insight into the way the assimilation procedure adjusts the sea-ice state is obtained from an analysis of sea ice evolution along an individual buoy trajectory (Figure 5). We choose buoy no. 24289, which has a drift track in the Chukchi Sea. For most of the buoy's lifetime, the simulated buoy trajectory with drift data assimilation lies between the true trajectory and the trajectory derived from the experiment without data assimilation. The zonal and meridional sea-ice velocities along the true buoy track (Figure 5, gray line) show a slight improvement due to the assimilation (Figure 6). Again, the satellite data and the model-only simulation are regarded as two possible solutions of the true sea-ice velocity and the assimilated velocities lie between them. Maxima of the observed velocity are better captured with the assimilation than in the model-only experiment. Due to the assimilation, the rmse for the zonal and meridional velocities with respect to the independent buoy data are reduced from 0.07 m/s to 0.05 m/s and from 0.07 m/s to

0.06 m/s, respectively. Correlations between simulated and observed velocities increase from 0.76 to 0.89 (zonal velocities) and 0.73 to 0.83 (meridional velocities).

3.2 Ice concentration

The evolution of ice concentration along the buoy track (Figure 7) reflects two phases: During the first month, ice concentrations between 0.8 and 0.95 prevail. Here, the SEIK analysis captures a good part of the observed variability. Absolute numbers underestimate the observed concentration, but in contrast to the experiment without data assimilation (represented by the 'FESIM' time series in Fig. 7), the course of minima and maxima is well reproduced. After about three weeks, thermodynamic ice growth (respresented as 'SEIK Forecast Change' in Figure 7) leads to an increase of ice concentration to values very close to 1. While this high concentration agress well with the observations, observed variability during this phase is not captured. It is clear that the upper limit of 1.0, which needs to be applied to the ice concentration variable in all Hibler-type sea-ice models, prevents the SEIK filter algorithm (which assumes a normal distribution of states!) from adjusting the ice concentration towards observed anomalies. Furthermore, winter conditions with rapid ice growth drive all model ensemble members into situations with very high ice concentrations, so that the ensemble variability and correlations with ice drift patterns are very small. However, although no ice concentration information is used in the assimilation procedure, the rms concentration error with respect to the SSM/I-derived concentration decreases from 0.05 (without assimilation) to 0.04.

To show that the SEIK analysis is able to improve the agreement between modeled and observed ice concentrations even for basin-scale fields, we compare three-daily mean sea-ice concentrations from simulations with and without data assimilation to satellite data from the same times and locations. Relative frequencies of ice concentration data pairs (clustered into 10% bins) are computed. Large frequencies in the diagonal elements in Figs. 8 and 9 represent a good match between model and observation.

For the Central Arctic (latitude $> 81°$ N) a clear improvement due to the assimilation of sea-ice drift is evident (Fig. 8, top). The relative frequency of ice concentrations between 0.9 to 1.0 coinciding for modeled and observed data increases from 0.69 (without assimilation) to 0.76. Correlation between modeled and observed sea-ice concentration in this region increases from 0.5 (without assimilation) to 0.6. The rms ice concentratin error decreases from 0.18 to 0.10.

For the Siberian Seas (including Chukchi, East Siberian, Laptev and Kara Seas), the relative frequency of agreement for the 0.9 to 1.0 ice concentration bin increases from 0.25 to 0.52 (Fig. 8, bottom), but the correlation coefficient between modeled and observed concentrations decreases from 0.7 to 0.6. On the other hand, the rms error for ice concentrations in this area decreases from 0.31 to 0.26.

In the Beaufort Sea, the assimilation process leads to an overestation of ice extent, which is reflected by a relatively high number of points with a simulated ice concentration near 100% where observations indicate little or no ice coverage (Fig. 9, top right). The reason for this is that velocity fields contain no information about the location of the ice egde. Furthermore, the region around the ice edge is a regime in which internal ice stress is very small or zero (so-called free drift regime). Here, the covariance between ice concentration or thickness (which are the dominant parameters determining the ice strength - c.f. Eq. 1) and ice drift is very small, so that the present filter setup is unable to achieve an appropriate correction of the sea ice state. We expect that additional assimilation of ice concentration data will easily cure this problem. In regions with a compact ice cover, the assimilation again leads to an improvement.

In the Greenland and Barents Seas the assimilation has little effect on sea-ice concentration (Fig.9, bottom). In contrast to the other regions, the agreement between simulation and observation weakens. Again this is a region where free drift situations prevail so that little covariance between ice thickness or concentration and drift can be found.

3.3 Ice Thickness

3.3.1 Connections and Covariance

The most sustainable modification during the assimilation procedure is the correction of ice thickness. It is achieved due to the covariances between ice thickness and ice drift, which are connected through the sea ice rheology. For a given momentum forcing (wind and ocean stress field), the resulting ice drift field is mainly determined by the occurence of internal stress, which in turn is dominated by the ice thickness distribution as described in Eq. (1) - provided the fraction A of open water is smaller than about 10%, which usually is the case inside the pack. Therefore, we obtain a high correlation between ice thickness and drift mainly in regions with a compact ice cover. If the model forcecast yields a drift estimate that is too fast compared to the observations, the analysis will correct this by modifying the ice thickness distribution in a way that the statistics have found to be suitable to correct the drift towards the observed state. The modified thickness distribution will then remain through the model forecast phase and consistently correct the drift. The biggest corrections occur during the first 2-4 assimilation cycles. After this initial adjustment phase, the corrected ice thickness field yields velocities that only need little updates towards the observations.

3.3.2 Comparison with submarine data

Compared to the model-only experiment, the sea-ice thickness pattern in the simulation with ice drift data assimilation is considerably different (Fig. 10). Generally, the ice is thicker; ice thickness at the North Pole has increased from 1.9 to 3.5 m. The ice thickness distribution in the assimilation experiment shows a pattern similar to the long-term mean autumn map of *Bourke and Garrett* (1987). For this particular snapshot, however, it is not obvious which distribution is more realistic.

We therefore use ice thickness data derived from a submarine ULS *Wensnahan and Rothrock* (2005); *NSIDC* (1998, updated 2006) for comparison (Fig. 10, center). These data have been recorded from 13-31 October 2000. They capture thicknesses from several centimeters up to 4 m.

The scatter plot (Fig. 11 left) reveals that the model alone is not able to reproduce the large observed ice thickness variability. Not only is the simulated thickness range smaller than the observed; the areas of mininium and maximum ice thicknesses do not even coincide. This is reflected by a rather small correlation coefficient $r = 0.24$. A least squares regression yields a slope of only 0.19 (where 1.0 would represent a perfect agreement).

Note that this deficiency is not a specific FESOM feature: *Stark et al.*

(2008) use the same ULS dataset and obtain similar results. In model-to-data comparisons by *Rothrock et al.* (2003), the agreement for individual submarine cruises is similarly poor. It appears that although large-scale sea-ice models for the Arctic capture the interannual thickness variability rather well, they fail to reproduce the observed thickness distribution on the scale of single cruise tracks.

In the simulation with velocity data assmimilation (Fig. 11, right), the agreement is much better with a correlation coefficient $r = 0.83$ and a regression slope of 1.26. Compared to the study of *Stark et al.* (2008), ice thickness modifications due to assimilation in our experiments are more severe. While in their case the model underestimates the maximum ice thickness before and after assimilation, assimilation tends to overestimate ice thickness in our case. We attribute this overestimation to the fact that the thickness variations applied by the SEIK filter only rely on statistical relations without any constraints regarding the absolute thickness values. With or without data assimilation, FESOM does not produce sea-ice thicknesses below 1 m on this ULS section. FESOM also overestimates the ice thickness in the western Beaufort and Chukchi Seas; compared to the model-only simulation with a regional mean ice thickness of 2-3 m, the assimilation still yields an improvement with a typical thickness of 1-2 m. However, the benefit of data assimilation in the FESOM simulations is that large parts of the oberserved cruise-scale thickness variability are now well captured; most of the areas of thin or thick ice now coincide.

3.3.3 Seasonal sea-ice thickness pattern change

The assimilation procedure modifies not only the mean thickness field, but also enables the model to reproduce the observed transition between summer and winter ice thickness distributions. While the simulated ice thickness distribution for the period 13 Oct - 18 Nov 2000 (Fig. 12, top left) closely resembles the summer pattern of *Bourke and Garrett* (1987), the periods 19 Nov - 30 Nov and 1 Dec - 9 Dec 2000 (Fig. 12, top middle and right) represent the transition to the observed mean winter distribution (again from *Bourke and Garrett* (1987)). This transition is not at all present in the model-only experiment (Fig. 12, bottom panels).

Note that the transition from summer to winter distribution occurs in a rather short time at the end of November within only three assimilation steps (i.e. nine days). In Section 3.1, we have demonstrated the adjustment of the simulated ice drift pattern towards the observed field for the beginning of December 2000 (Figure 4). In contrast to the observations, the model-only experiment features a strong recirculation of sea ice along the northern Greenland and Canadian coast. The assimilation produces a larger sea-ice thickness at the Canadian coast (Fig. 12, top panels), which results in a higher ice strength and in a higher resistance of the ice towards deformation by air and ocean stress. While this does not lead to a complete elimination of the recirculation, the drift along the Candadian Archipelago is still substantially reduced. Due to the global covariance matrix used, this also affects the course of the transpolar drift stream and thus the major ice export pathway.

4 Discussion and conclusions

We have presented a finite-element sea-ice model in a regional configuration covering the entire Arctic Ocean. The SEIK filter has been used for the sea-ice drift data assimilation. The filter uses the ensemble-derived cross-covariances between the ice thickness/concentration and the ice drift in order to obtain a sustainable drift correction, and at the same time to modify the ice thickness and concentration fields. In this setup, the drift is improved due to the modifications of the more conservative variables sea-ice concentration and thickness. These are the variables that (for a given velocity field) define the internal stress, and thus the resistance of ice to deformation. The modified thickness distribution then feeds back to modify ice drift field.

Our results indicate that by using the SEIK filter we have been able to improve not only the single observed variable, but the complete model state.

In our case, the assimilation of observed sea-ice drift fields not only corrects the ice drift, but also improves the ice thickness distribution. Given that observed ice thickness fields are not available over the entire Arctic area and on a regular basis, this feature promises to provide a tool for obtaining, e.g., initial ice thickness fields for operational ice forecasts, as are envisaged for optimization of ship routes in the Arctic Ocean. Since the modeled ice concentration is in good agreement with observations already in stand alone simulations, it is not surprising that the improvement due to the data assimilation is modest. The main discrepancies between the analysis and the data used for validation occur near the ice edge. This, however, is a regime of predominantly free drift, so that the cross-correlations between the ice drift and the thickness/concentration are weak. In this regime, our approach is unable to yield a significant improvement. In order to improve the results near the ice edge, simultaneous assimilation of the ice concentration would need to be performed.

While the simulated ice concentration is limited to values between 0 and 1, the ice thickness is only weakly constrained in the model. The ice drift data assimilation improves the sea-ice thickness pattern, mainly by increasing the spatial variability to a realistic magnitude. However, an overestimation of the sea-ice thickness seems to be a consistent feature in our assimilation experiments. Given that the modification of the ice thickness is the main mechanism for a sustainable drift correction in our setup, and that no ice thickness data are used to constrain the analyzed thickness fields so far, we expect that providing even scarcely distributed ice thickness information in addition to the ice drift information, and/or a different choice of the ice strength parameter P^*, will alleviate this problem.

Acknowledgments

We would like to thank Dr. Lars Nerger and Dr. Michael Schröter for their help and support. Sea ice velocities and concentration data used in this study were obtained from CERSAT, at IFREMER, Plouzané (France). The NCEP/NCAR reanalysis data were provided by the NOAA Climate Diagnostics Center, Boulder, online at http://www.cdc.noaa.gov. Some of the model experiments utilized resources from the North German Alliance for the Advancement of High-Performance Computing (HLRN). This work was partly funded by the EU project SITHOS (EVK2-2002-00146).

References

Arbetter, T., A. Lynch, J. Maslanik, and W. Meier, Effects of data assimilation of ice motion in a basin-scale sea ice model, in *Ice in the Environment:*

Proceedings of the 16th IAHR International Symposium on Ice, edited by V. Squire and P. Langhore, pp. 186–193, International Association of Hydraulic Engineering and Research, Dunedin, New Zeeland, 2-6 December 2002, 2002.

Bourke, R. H., and R. P. Garrett, Sea ice thickness distribution in the Arctic Ocean, *Cold Reg. Sci. Technol.*, *13*, 259–280, 1987.

Comiso, J. C., D. J. Cavalieri, C. L. Parkinson, and P. Gloersen, Passive microwave algorithms for sea ice concentration: A comparison of two techniques, *Remote Sens. Environ.*, *12*(60), 357–384, 1997.

Dai, M., T. Arbetter, and W. Meier, Data assimilation of sea-ice motion vectors: Sensitivity to the perameterization of sea-ice strength, *Ann. Glaciol.*, *44*, 357–360, 2006.

Dulière, V., On the assimilation of ice velocity and concentration data into large-scale sea ice models, Ph.D. thesis, Université catholique de Louvain, Faculté des sciences, École doctorale en géosciences, 2007.

Dulière, V., and T. Fichefet, On the assimilation of ice velocity and concentration data into large-scale sea ice models, *Ocean Sci.*, *3*, 321–335, 2007.

Ebert, E. E., and J. A. Curry, An intermediate one-dimensional thermodynamic sea ice model for investigating ice-atmosphere interactions, *J. Geophys. Res.*, *98*(C6), 10,085–10,109, 1993.

Ezraty, R., and J. F. Piollé, *Sea Ice Drift in the Central Arctic Combining Quikscat and SSM/I Sea Ice Drift Data User's Manual 1.0*, Laboratoire d'Océanographie Spatiale, Département d'Océanographie Physique et Spatiale IFREMER/ Centre de Brest, 2004a.

Ezraty, R., and J. F. Piollé, *Sea-Ice Drift in the Central Arctic Estimated from SeaWinds/Quikscat Backscatter Maps User's Manual **2.1***, Laboratoire d'Océanographie Spatiale, Département d'Océanographie Physique et Spatiale IFREMER/ Centre de Brest, France, 2004b.

Fischer, H., *Vergleichende Untersuchungen eines optimierten dynamisch-thermodynamischen Meereismodells mit Beobachtungen im Weddellmeer*, *Berichte zur Polarforschung*, vol. 166, Alfred Wegener Institute (AWI), Bremerhaven, Germany, 1995.

Gibson, J. K., P. Kållberg, S. Uppala, A. Hernandez, and E. Serrano, *ERA Description. Re-Analysis (ERA) Project Report, Series 1*, European Centre for Medium-Range Weather Forecast (ECMWF), Shinfield Park, 1997.

Harder, M., and H. Fischer, Sea ice dynamics in the Weddell Sea simulated with an optimized model, *J. Geophys. Res.*, *104*(C5), 11,151–11,162, 1999.

Hibler, W. D., A Dynamic Thermodynamic Sea Ice Model, *J. Phys. Oceanogr.*, *9*(4), 815–864, 1979.

Hunke, E. C., and J. K. Dukowicz, An Elastic-Viscous-Plastic Model for Sea Ice Dynamics, *J. Phys. Oceanogr.*, *27*(9), 1849–1867, doi:10.1175/1520-0485(1997)027, 1997.

Kaleschke, L., Fernerkundung des Meereises mit passiven und aktiven Mikrowellensensoren, Ph.D. thesis, Fachbereich 1 (Physik/Elektrotechnik), Universität Bremen, 2003.

Kaleschke, L., C. Lüpkes, T. Vihma, J. Haarpaintner, A. Borchert, J. Hartmann, and G. Heygster, SSM/I sea ice remote sensing for mesoscale ocean-atmosphere interaction analysis, *Canadian Journal of Remote Sensing*, *27*(5), 526–537, 2001.

Kalnay, E., M. Kanamitsu, R. Kistler, W. Collins, D. Deaven, L. Gandin, M. Iredell, S. Saha, G. White, J. Woolen, Y. Zhu, M. Chelliah, W. Ebisuzaki, W. Higgins, J. Janowiak, K. C. Mo, C. Ropelewski, J. Wang, A. Leetmaa, R. Reynolds, R. Jenne, and D. Josephs, The NCEP/NCAR 40-Year Reanalysis Project, *Bull. Amer. Meteorol. Soc.*, *77*(3), 437–471, 1996.

Kistler, R., E. Kalnay, W. Collins, S. Saha, G. White, J. Woollen, M. Chelliah, W. Ebisuzaki, M. Kanamitsu, V. Kousky, H. van den Dool, R. Jenne, and M. Fiorino, The NCEP-NCAR 50-Year Reanalysis: Mothly Means CD-ROM and Documentation, *Bull. Amer. Meteorol. Soc.*, *82*(2), 247–268, 2001.

Kreyscher, M., *Dynamics of Arctic sea ice - Validation of different rheology schemes for the use in climate models*, *Reports on Polar Research*, vol. 291, Alfred Wegener Institute (AWI), Bremerhaven, Germany, 1998.

Leppäranta, M., A growth model for black ice, snow ice and snow thickness in subarctic basins, *Nordic Hydrology*, *14*(2), 59–70, 1983.

Lieser, J. L., *A Numerical Model for Short-term Sea Ice Forecasting in the Arctic*, *Reports on Polar and Marine Research*, vol. 485, Alfred Wegener Institute (AWI), Bremerhaven, Germany, 2004.

Lindsay, R., J. Zhang, and D. Rothrock, Sea ice deformation rates from measurements and in a model, *Atmos. Ocean*, *40*, 35–47, 2003.

Lisæter, K., G. Evensen, and S. Laxon, Assimilating synthetic cryosat sea ice thickness in a coupled ice-ocean model, *Journal of Geophysical Research*, *112*(C07023), doi:10.1029/2006JC003786, 2007.

Lisæter, K. A., J. Rosanova, and G. Evensen, Assimilation of ice concentration in a coupled ice-ocean model using ensemble kalman filter, *Ocean Dynamics*, *53*, 368–388, 2003.

Martin, T., *Arctic Sea Ice Dynamics: Drift and Ridging in Numerical Models and Observations*, *Reports on Polar and Marine Research*, vol. 563, Alfred Wegener Institute (AWI), Bremerhaven, Germany, 2007.

Meier, W. N., and J. A. Maslanik, Synoptic-scale ice-motion case-studies using assimilated motion fields, *Ann. Glaciol.*, *33*, 145–150, 2001a.

Meier, W. N., and J. A. Maslanik, Improved sea ice parcel trajectories in the Arctic via data assimilation, *Mar. Pollut. Bull.*, *42*, 506–512, 2001b.

Meier, W. N., and J. A. Maslanik, Effect of environmental conditions on observed, modeled, and assimilated sea ice motion errors, *J. Geophys. Res.*, *108*(C5), doi:10.1029/2002JC001333, 2003.

Meier, W. N., J. A. Maslanik, and C. W. Fowler, Error analysis and assimilation of remotely sensed ice motion within an Arctic sea ice model, *J. Geophys. Res.*, *105*(C2), 3339–3356, doi:10.1029/1999JC900268, 2000.

NSIDC, *Submarine upward looking sonar ice draft profile data and statistics*, Boulder, CO: National Snow and Ice Data Center/World Data Center for Glaciology. Digital media, 1998, updated 2006.

Ortmeyer, M., and I. Rigor, International Arctic Buoy Programme Data Report 1 January 2003 - 31 December 2003, *Technical Memorandum APL - UW TM 2-04*, Applied Physics Laboratory, University of Washington, http://iabp.apl.washington.edu, 2004.

Owens, W., and P. Lemke, Sensitivity studies with a sea ice-mixed layer pycnocline model in the weddel sea, *J. Geophys. Res.*, *95*(C6), 9527–9538, 1990.

Pacanowski, R., and S. Philander, Parameterization of vertical mixing in numerical models of the tropical oceans, *Journal of Physical Oceanography*, *11*, 1443–1451, 1981.

Parkinson, C. L., and W. M. Washington, A large-scale numerical model of sea ice, *J. Geophys. Res.*, *84*(C1), 311–337, 1979.

Pham, D. T., Stochastic Methods for Sequential Data Assimilation in Strongly Nonlinear Systems, *Mon. Weather Rev.*, *129*, 1194–1207, 2001.

Pham, D. T., J. Verron, and L. Gourdeau, Singular evolutive Kalman filters for data assimilation in oceanography, *C. R. Acad. Sci. Ser. II*, *326*(4), 255–260, 1998.

Rigor, I., Iabp drifting buoy, pressure, temperature, position, and interpolated ice velocity, Compiled by the Polar Science Center, Applied Physics

Laboratory, University of Washington, Seattle, in association with NSIDC. Boulder, CO: National Snow and Ice Data Center. Digital media, 2002.

Rothrock, D. A., J. Zhang, and Y. Yu, The arctic ice thickness anomaly of the 1990s: A consistent view from observations and models, *J. Geophys. Res.*, *108*(C3), doi:10.1029/2001JC001208, 2003.

Semtner, A. J., A model for the thermodynamic growth of sea ice in numerical investigations of Climate, *J. Phys. Oceanogr.*, *6*, 409–425, 1976.

Stark, J., J. Ridley, M. Martin, and A. Hines, Sea ice concentration and motion assimilation in a sea ice–ocean model, *Journal of Geophysical Research*, *113*, C05S91, doi:10.1029/2007JC004224, 2008.

Thomas, D., and D. Rothrock, Blending Sequential Scanning Multichannel Microwave Radiometer and buoy data into a sea ice model, *J. Geophys. Res.*, *94*, 10,907–10,920, 1989.

Thomas, D., and D. Rothrock, The Arctic Ocean ice balance: a Kalman smoother estimate, *J. Geophys. Res.*, *98*, 10,053–10,067, 1993.

Thomas, D., S. Martin, and M. Steele, Assimilating satellite concentration data into an Arctic sea ice mass balance model, *J. Geophys. Res.*, *101*, 20,849–20,868, 1996.

Timmermann, R., S. Danilov, J. Schröter, C. Böning, and K. Rollenhagen, On the representation of high latitudes in a finite-element global sea ice – ocean model, *Ocean Modelling*, (submitted), 2008.

Vowinckel, E., and S. Orvig, The Climate of the North Polar Basin, in *Climates of the polar regions*, vol. 14, edited by S. Orvig, pp. 401–424, World Survey of Climatology, New York, 1970.

Wensnahan, M., *Submarine upward looking sonar ice draft profile data and statistics: Documentation for G01360 Analog Subset*, National Snow and Ice Data Center, http://nsidc.org/data/docs/noaa/g01360_upward_looking_sonar/index.html, 2006.

Wensnahan, M., and D. Rothrock, Sea-ice draft from submarine-based sonar: Establishing a consistent record from analog and digitally recorded data, *Geophys. Res. Lett.*, *32*, doi:10.1029/2005GL022507, 2005.

Zhang, J., D. R. Thomas, D. A. Rothrock, R. W. Lindsay, Y. Yu, and R. Kwok, Assimilation of ice motion observations and comparisons with submarine ice thickness data, *J. Geophys. Res.*, *108*(C6), doi: 10.1029/2001JC001041, 2003.

Figure 1: The FESIM domain, indicated by the black rectangle, covers the Arctic Ocean, its marginal seas, and part of the North Atlantic.

Figure 2: Buoy trajectories in the Chukchi and Beaufort Seas from the year 2000. Assimilation (black line), FESIM model only (dark grey line) and true buoy trajectory (light grey line). (a) buoy no. 24289 (c.f. Figure 5).

Figure 3: Three-day mean sea-ice velocities along buoy trajectories in the Arctic in autumn 2000. No satellite-derived drift data were available for assimilation during a period of nine days in November.

Figure 4: Arctic sea-level pressure and sea-ice drift patterns averaged from 1 to 9 December 2000. Top left: NCEP reanalysis sea-level pressure, top right: model-only simulation, bottom left: observed drift, bottom right: model with drift data assimilation.

Figure 5: Buoy trajectory of buoy no. 24289, located in the Chukchi Sea. Assimilation (thick black line), model-only (black line) and true buoy trajectory (gray line).

Figure 6: Three-day mean zonal (top) and meridional (bottom) velocity along the trajectory of buoy no. 24289: assimilation (solid, black), model-only (thin solid, black), satellite observation (dashed, gray) and buoy no.

24289 (solid, gray).

Figure 7: Sea ice concentration along the trajectory of buoy no. 24289: assimilation (solid, black), model-only (thin solid, black), accumulated SEIK analysis change (solid gray), accumulated SEIK forecast change (dashed, gray), SSM/I concentration (dashed, black)

Figure 8: Modeled vs. observed sea-ice concentration data: probability density for 13 - 31 October 2000; reference (left) and assimilation (right) results for the Central Arctic (latitude $> 81^\circ$ N, top) and Siberian Seas (bottom, including Chukchi, East Siberian, Laptev and Kara Sea).

Figure 9: Modeled vs. observed sea-ice concentration data: probability density for 13 - 31 October 2000; reference (left) and assimilation (right) results for the Greenland and Barents Seas (top), and the Beaufort Sea (bottom).

Figure 10: Mean sea-ice thickness [m] from 13 - 31 October 2000: Model-only simulation (a), ULS-derived thickness observation (b) and assimilation (c).

Figure 11: Scatter plot of modeled vs. observed sea-ice thickness without (left) and with (right) assimilation for the observation period from 13 - 31 October 2000.

Figure 12: Simulated sea-ice thickness maps [m] for autumn 2000 in the assimilation experiment (top) and in the model-only simulation (bottom).

Figure 1: The FESIM domain, indicated by the black rectangle, covers the Arctic Ocean, its marginal seas, and part of the North Atlantic.

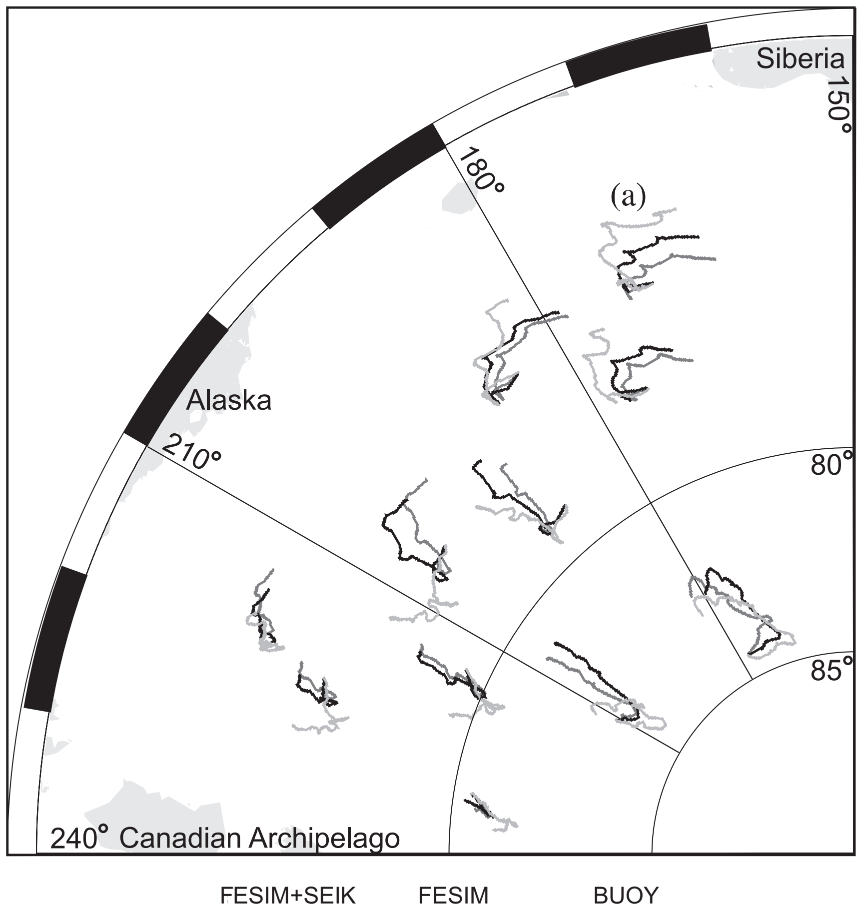

Figure 2: Buoy trajectories in the Chukchi and Beaufort Seas from the year 2000. Assimilation (black line), FESIM model only (dark grey line) and true buoy trajectory (light grey line). (a) buoy no. 24289 (c.f. Figure 5).

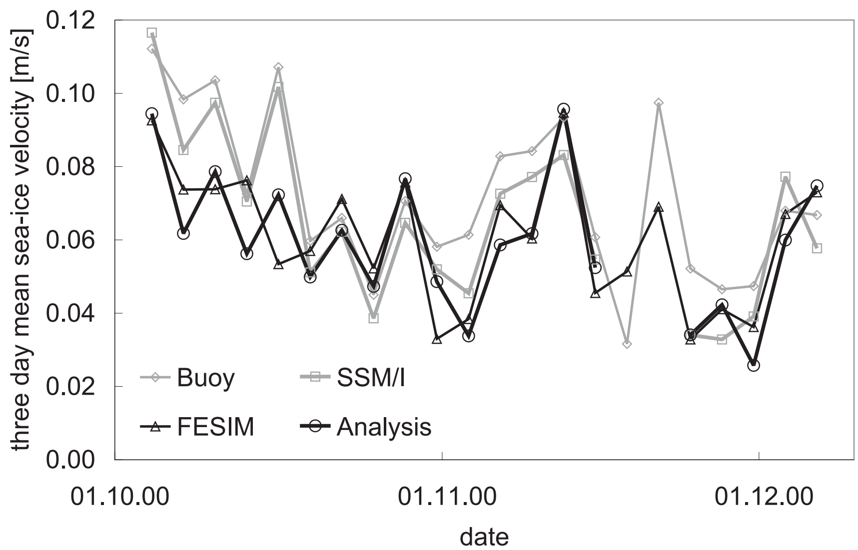

Figure 3: Three-day mean sea-ice velocities along buoy trajectories in the Arctic in autumn 2000. No satellite-derived drift data were available for assimilation during a period of nine days in November.

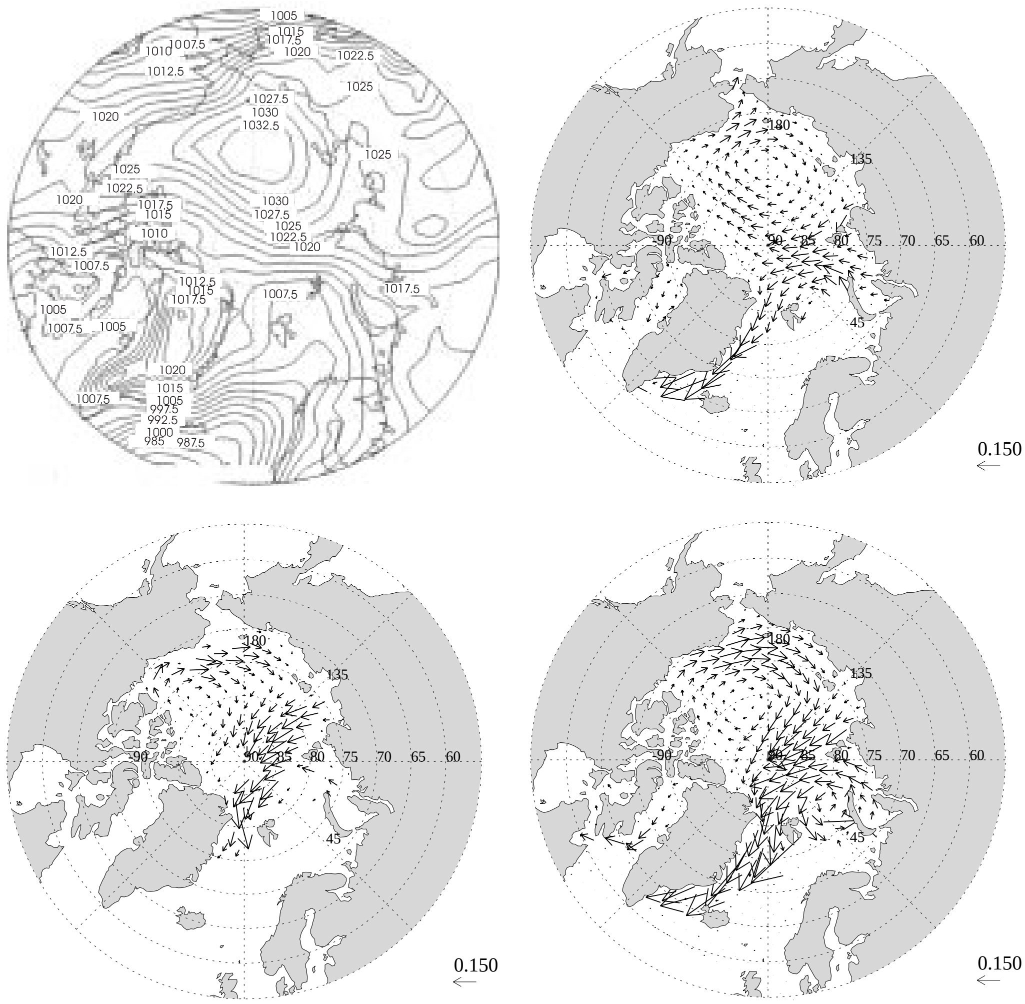

Figure 4: Arctic sea-level pressure and sea-ice drift patterns averaged from 1 to 9 December 2000. Top left: NCEP reanalysis sea-level pressure, top right: model-only simulation, bottom left: observed drift, bottom right: model with drift data assimilation.

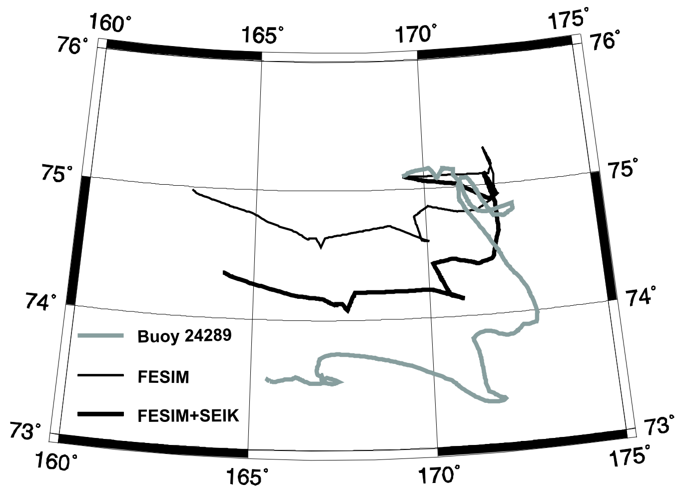

Figure 5: Buoy trajectory of buoy no. 24289, located in the Chukchi Sea. Assimilation (thick black line), model-only (black line) and true buoy trajectory (gray line).

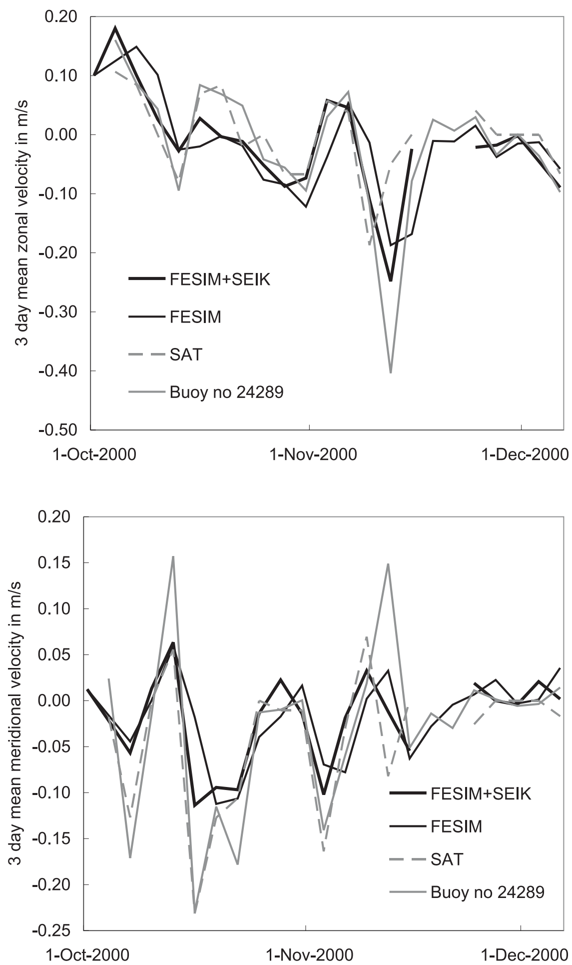

Figure 6: Three-day mean zonal (top) and meridional (bottom) velocity along the trajectory of buoy no. 24289: assimilation (solid, black), model-only (thin solid, black), satellite observation (dashed, gray) and buoy no. 24289 (solid, gray).

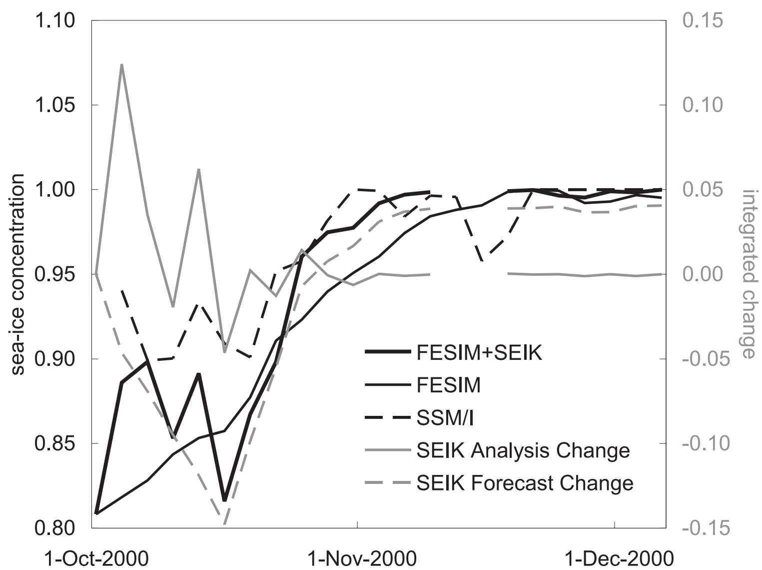

Figure 7: Sea ice concentration along the trajectory of buoy no. 24289: assimilation (solid, black), model-only (thin solid, black), accumulated SEIK analysis change (solid gray), accumulated SEIK forecast change (dashed, gray), SSM/I concentration (dashed, black)

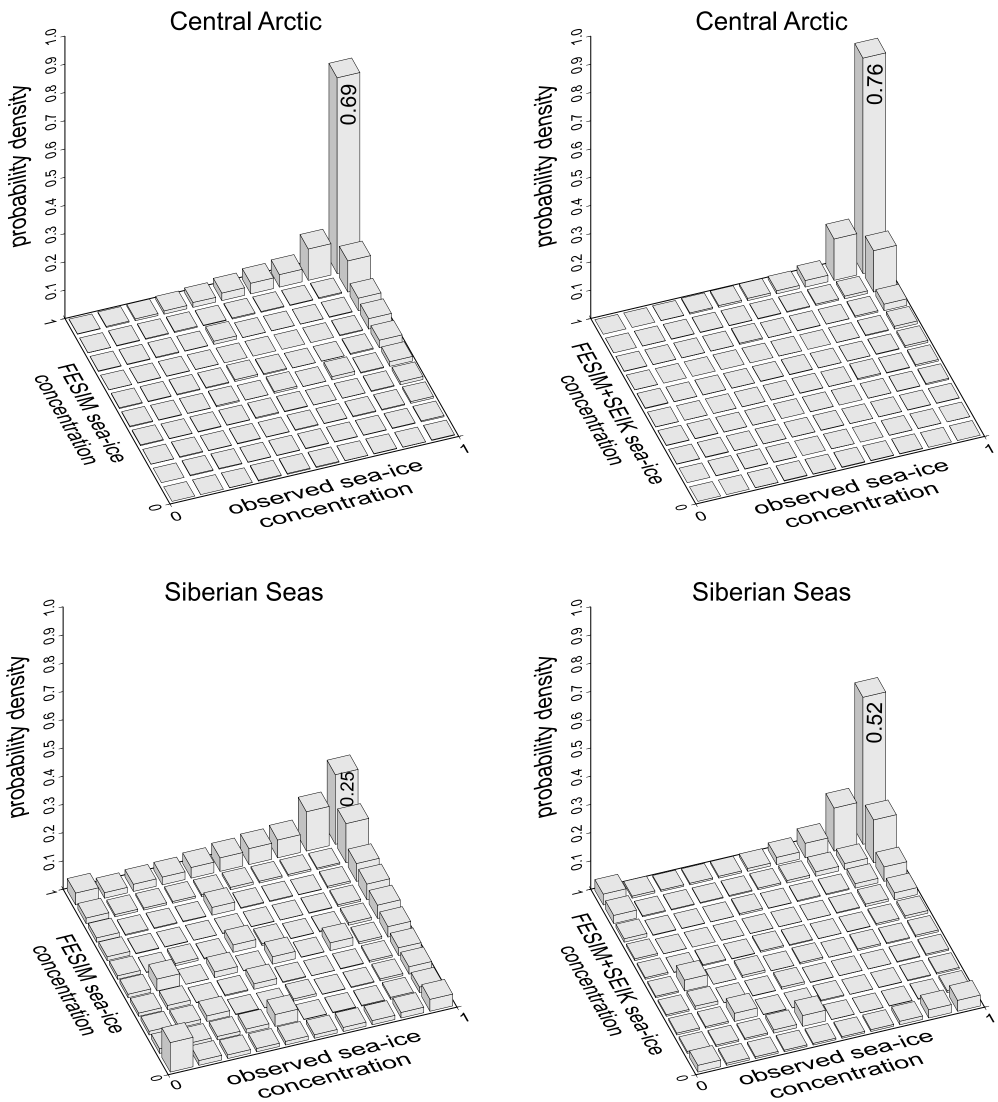

Figure 8: Modeled vs. observed sea-ice concentration data: probability density for 13 - 31 October 2000; reference (left) and assimilation (right) results for the Central Arctic (latitude $> 81^\circ$ N, top) and Siberian Seas (bottom, including Chukchi, East Siberian, Laptev and Kara Sea).

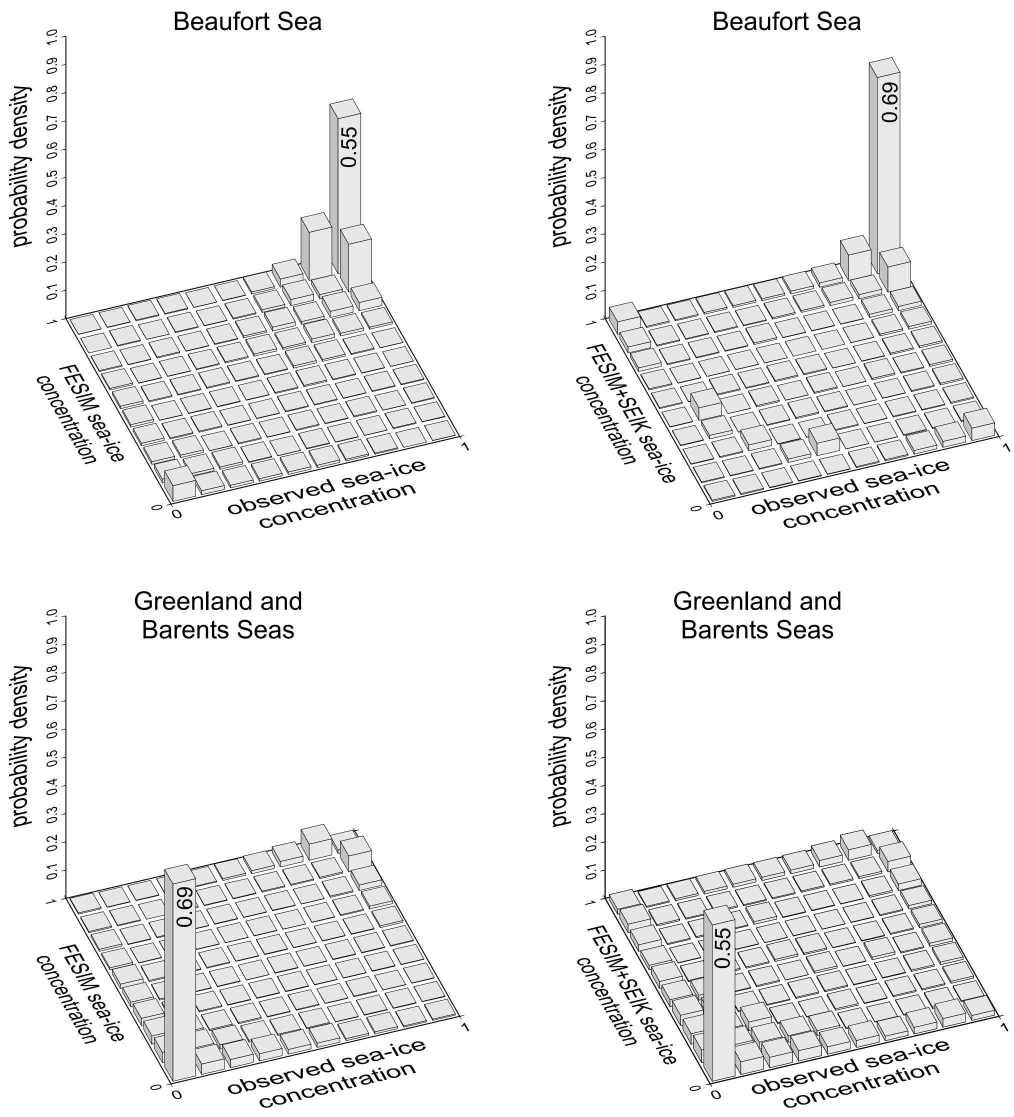

Figure 9: Modeled vs. observed sea-ice concentration data: probability density for 13 - 31 October 2000; reference (left) and assimilation (right) results for the Greenland and Barents Seas (top), and the Beaufort Sea (bottom).

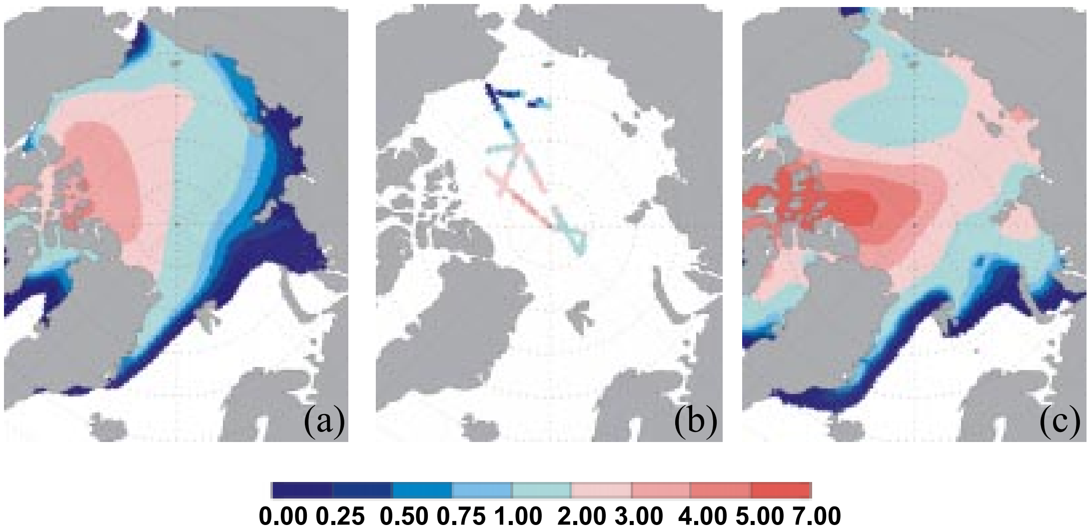

Figure 10: Mean sea-ice thickness [m] from 13 - 31 October 2000: Model-only simulation (a), ULS-derived thickness observation (b) and assimilation (c).

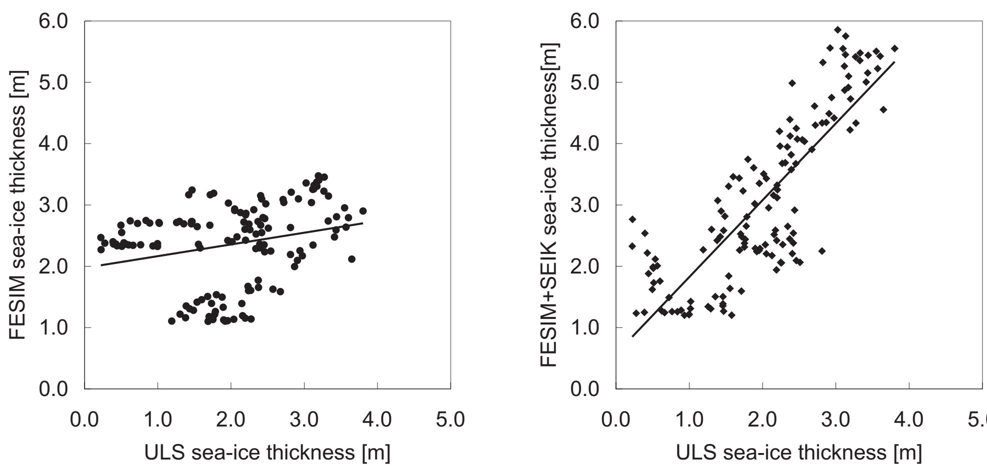

Figure 11: Scatter plot of modeled vs. observed sea-ice thickness without (left) and with (right) assimilation for the observation period from 13 - 31 October 2000.

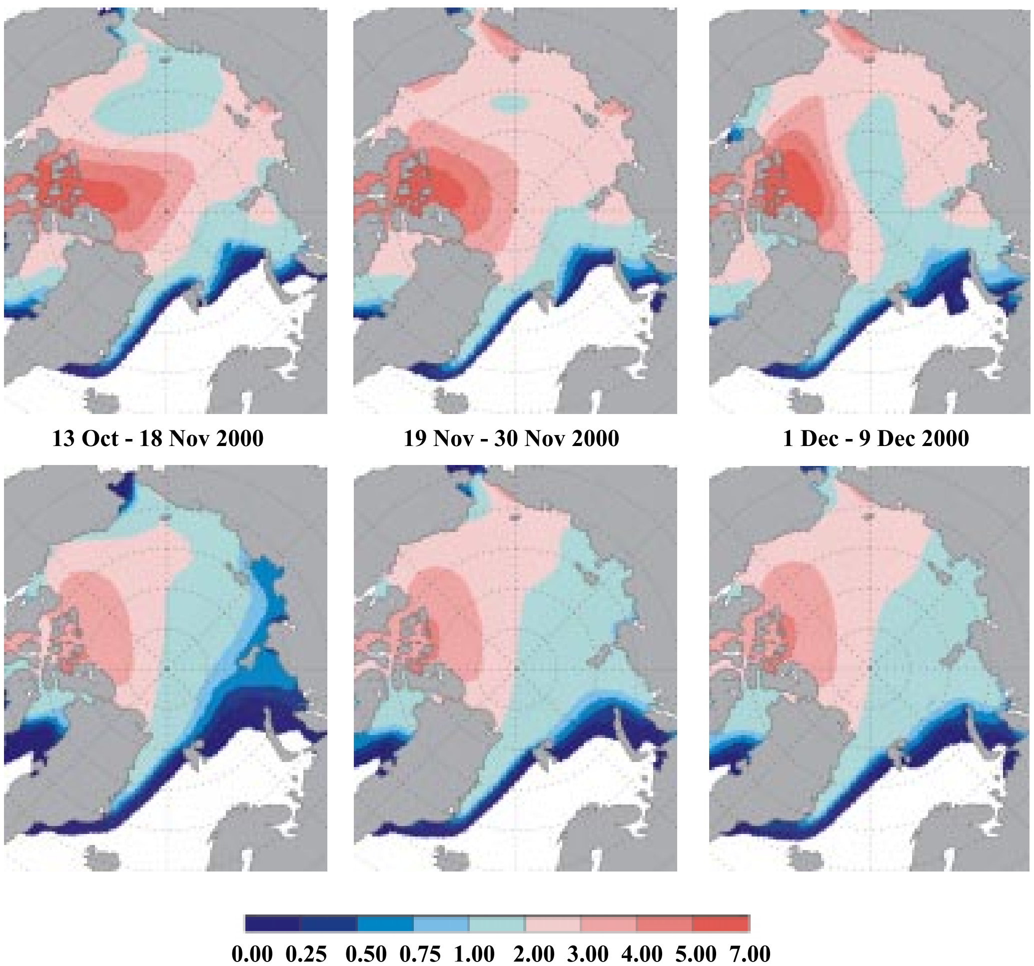

Figure 12: Simulated sea-ice thickness maps [m] for autumn 2000 in the assimilation experiment (top) and in the model-only simulation (bottom).